Kato Yuko (M2)
08/07/23

Olefin Transition-Metal Complex for Cross-Coupling Reactions

+ contents

1) Introduction
2) Nature of transition-metal olefin complex
3) Effects of olefin on transition-metal-catalysed reactions
 a) oxidative addition
 b) reductive elimination vs β-elimination
 c) stabilization of catalyst
 d) catalyst cycle including insertion to additive olefin (Appendix)
 e) olefins in substrates
 f) chiral diene ligands

Review : *ACIE* **2008**, *47*, 840.

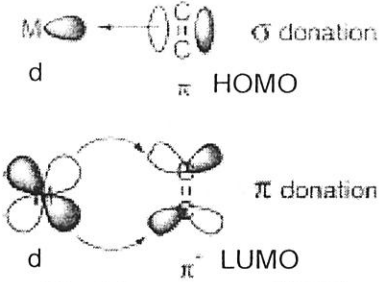

Fig 1. Dewar-Chatt-Duncanson (DCD) model for metal-olefin binding

1) Introduction

First reported transition-metal olefin complex.

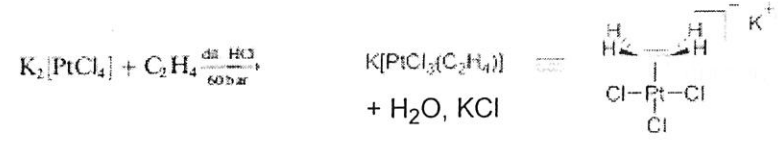

Zeise's salt (1827)

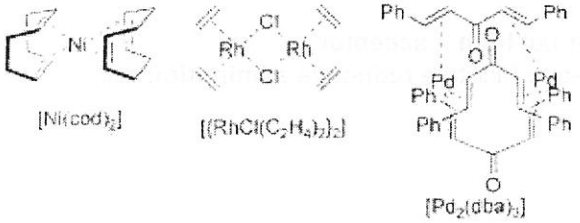

Stable but ligands are easily displaced by other ligands.
⟹ **Precursors for various cross-coupling reactions.**

Fig 2. Commercially available transition-metal olefin complex.

2) Nature of transition-metal olefin complex

- Transition-metal olefin bond is derived from σ-donation (olefin-to-metal) and π-donation (metal-to-olefin) (Fig 1)
- π-donation increases with the principal quantum number of the metal center.
  → The stabilities of complexes increases in this trend.

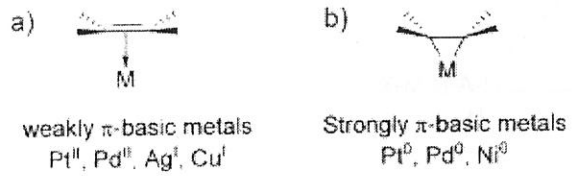

weakly π-basic metals
Pt^{II}, Pd^{II}, Ag^{I}, Cu^{I}

Strongly π-basic metals
Pt^{0}, Pd^{0}, Ni^{0}

Fig 3. Metal-binding model

22 Ti チタン 47.88	23 V バナジウム 50.94	24 Cr クロム 52.00	25 Mn マンガン 54.94	26 Fe 鉄 55.85	27 Co コバルト 58.93	28 Ni ニッケル 58.69	29 Cu 銅 63.55	30 Zn 亜鉛 65.39*
40 Zr ジルコニウム 91.22	41 Nb ニオブ 92.91	42 Mo モリブデン 95.94	43 Tc テクネチウム (99)	44 Ru ルテニウム 101.1	45 Rh ロジウム 102.9	46 Pd パラジウム 106.4	47 Ag 銀 107.9	48 Cd カドミウム 112.4
72 Hf ハフニウム 178.5	73 Ta タンタル 180.9	74 W タングステン 183.8	75 Re レニウム 186.2	76 Os オスミウム 190.2	77 Ir イリジウム 192.2	78 Pt 白金 195.1	79 Au 金 197.0	80 Hg 水銀 200.6

Fig 4. Periodic table

Table 1: CDA analyses for some HAu-L complexes (DFT, B3LYP, basis set II[36b])

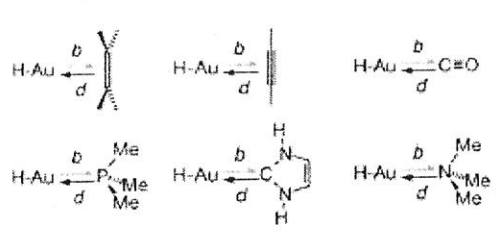

L	*d*	*b*	*d*/*b*
C_2H_4	0.36	0.13	2.9
C_2H_2	0.16	0.12	1.3
CO	0.27	0.22	1.2
PMe_3	0.53	0.16	3.3
imidazol-2-ylidene	0.36	0.12	3.0
NMe_3	0.20	0.01	32.7

CDA : charge decomposition analysis

Table 2: ETS analyses for HAu-L complexes (DFT, B3LYP, basis set II[36b]). All energies are in kcal mol^{-1}.

L	ΔE_{int}	ΔE_{Pauli}	ΔE_{elstat}	ΔE_{orb}
C_2H_4	−27.6	116.5	−90.9	−53.2
C_2H_2	−26.6	118.5	−91.4	−53.8
CO	−34.2	154.2	−120.3	−68.1
PMe_3	−43.8	153.5	−144.3	−53.0
imidazol-2-ylidene	−52.7	174.1	−173.3	−53.5
NMe_3	−29.9	82.5	−81.7	−30.7

$$\Delta E_{int} = \Delta E_{Pauli} + \Delta E_{elstat} + \Delta E_{orb}$$

ΔE_{int} : The binding energy.
ΔE_{Pauli} : The Pauli repulsion.
ΔE_{elstat} : The electrostatic attraction.
ΔE_{orb} : The orbital interaction.
ETS : extended transition state

○Substituent effect

Late transition metal

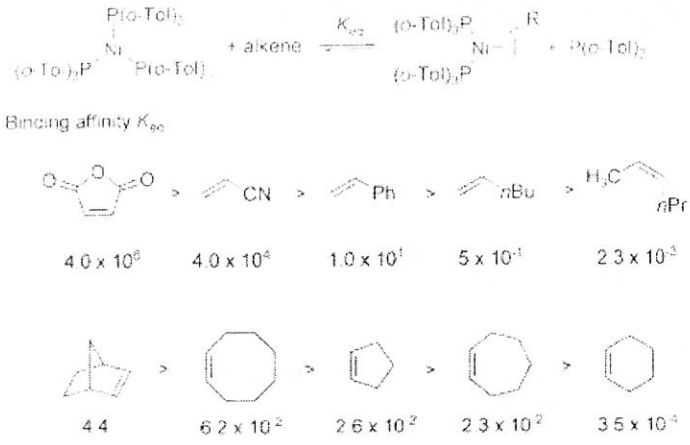

Scheme 4. Binding affinities of substituted and cyclic olefins to a Ni^0 complex. *o*-Tol = *ortho*-tolyl.

+ The **stronger** binding affinity, the **lower electron density** of olefin.
+ In cyclic olefins, the relief of ring strain affect the binding.
+ ***cis*** olefins bind more tightly than *trans* isomers.

Early transition metal

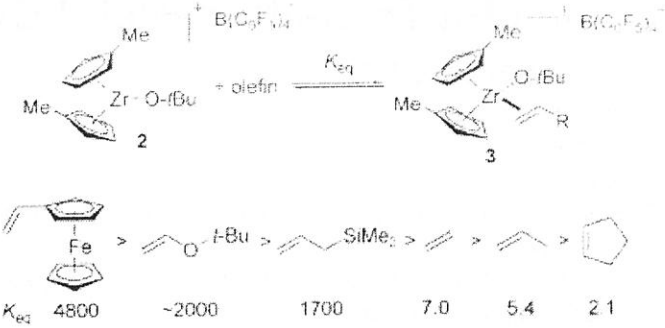

Scheme 6. Equilibrium constants of olefin coordination to a d^0 Zr^{IV} complex.

+ More **electron-rich** olefin bind more tightly.

○Effect on metal center

+ Strong **trans effect** derived from the nature of **weak σ donor** but **high π acceptor**.
+ Decreasing the electron density of metal center, and expected to facilitate **reductive elimination** but decelerate **oxidative addition**.

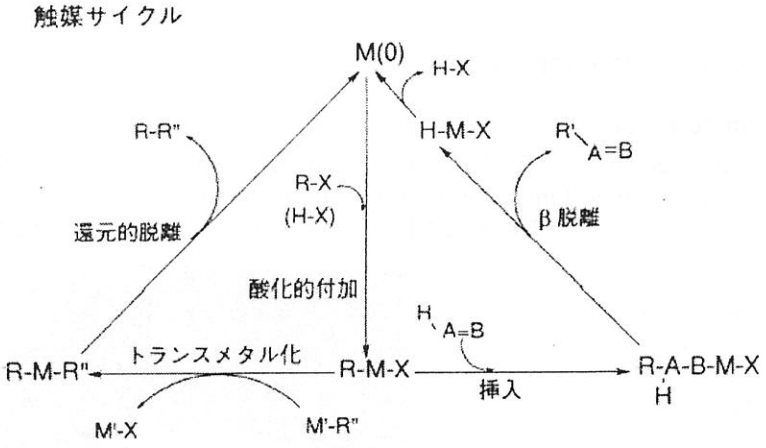

3) Effects of olefin on transition-metal-catalysed reactions

a) oxidative addition

Dba effect in oxidative addition using $Pd(dba)_2$ and PPh_3 (Amatore, Jutand et al. *Organometallics* **1993**, *12*, 3168.)

$Pd(dba)_2 \rightarrow Pd(dba) + dba$

unreactive

dba = *trans, trans*-dibenzylideneacetone

$Pd(dba) + 2PPh_3 \rightarrow Pd(dba)(PPh_3)_2$

$Pd(dba)(PPh_3)_2 \rightleftharpoons Pd(PPh_3)_2 + dba$ (K_1)

reactive

+ $K_0 = K_1K_2 = 0.14$ (The second dba is not labile and its deligation requires at least 8 equiv of PPh_3.)
+ When $Pd(dba)_2$ and 2 or 4 equiv of PPh_3 are used, the oxidative addition is **slower** than $Pd(PPh_3)_4$.
+ Substituted dba affect the rate of oxidative addition. (Scheme 11)

$\Rightarrow$ The rate of oxidative addtion is determined by the rate of **deligation** of of dba.

$Pd(PPh_3)_2 + PPh_3 \rightleftharpoons Pd(PPh_3)_3$ (K_2)

$Pd(dba)(PPh_3)_2 + PPh_3 \rightleftharpoons Pd(PPh_3)_3 + dba$ (K_0)

oxidative addition

$Pd(PPh_3)_2 + PhI \rightarrow PhPdI(PPh_3)_2$

14-electron complex

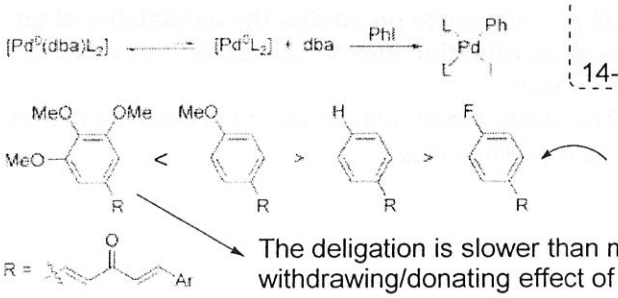

The deligation is slower than mono methoxy substitied dba due to the competing electron-withdrawing/donating effect of *m*-, *p*- methoxy group.

Scheme 11. Relative reaction rate for oxidative addition of substituted $[Pd(dba)_2]$ complexes. L = PPh_3.

Olefin as substrate may **inhibit** the generation of active 14-electron complex.

Heck reaction (Amatore , Jutand et al. *Organometallics* **2002**, *21*, 4540.)

$$Pd^0(PPh_3)_4 + PhI \xrightarrow{k_{app},\ R} PhPdI(PPh_3)_2 + 2\,PPh_3$$

Scheme 4. Mechanism of the Oxidative Addition of PhI to $Pd^0(PPh_3)_4$ in the Presence of an Alkene (R = Ph, CO_2Me)

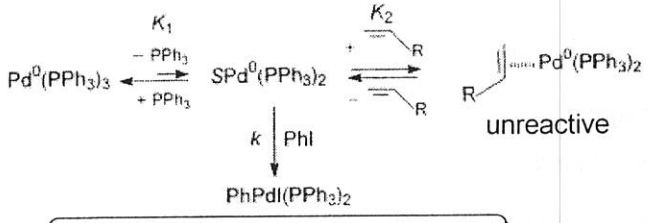

$$\frac{1}{k_{app}} = \frac{[L]}{kK_1} + \frac{K_2[RCH{=}CH_2]}{k}$$

$$Pd^0(PPh_3)_3 + \text{olefin} \underset{K_0 = K_1K_2}{\overset{K_0}{\rightleftharpoons}} \text{olefin-}Pd^0(PPh_3)_2 + PPh_3$$

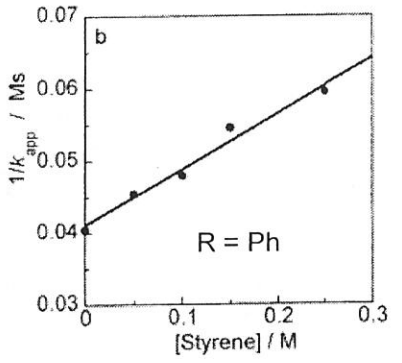

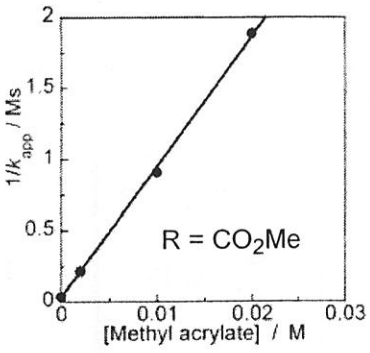

K_0 (R = Ph, styrene) = **4.8×10^{-3}**, K_0 (R = CO_2Me, methyl acrylate) = **7.5**

+ The higher concentration of olefin, the slower rate of oxidative addition.
+ The olefin with higher affinity to Pd(0) (methyl acrylate) affect the rate of oxidative addition.
+ This deceleration is observed also in Sonogashira rxn (*Eur. J. Org. Chem.* **2004**, 366.), Stille rxn (*JACS* **2003**, *125*, 4212.).

b) reductive elimination

Reductive elimination vs β–elimination (Sustmann et al. *TL* **1986**, *27*, 5207.)

Scheme 43. Palladium-catalyzed coupling of benzyl bromide with tetramethylstannane. HMPA = hexamethylphosphoramide.

+ No β-hydrogen substrate.
+ Pd cat : [Pd(bipy)Et_2] gave quantitative yield.
+ In the presence of catalytic fumaronitrile (3 equiv relative to Pd) or Pd cat : [Pd-(bipy)(fumaronitrile)] (1.5 mol%) gave slightly lower yield than only [Pd(bipy)Et_2].

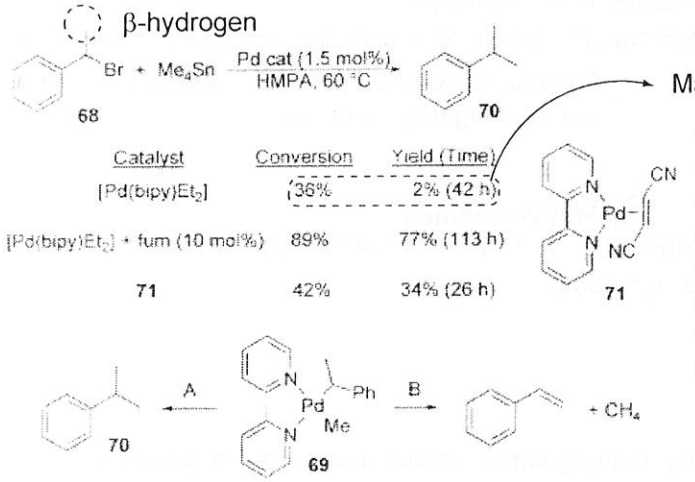

Main product was **styrene** from β–**elimination** (path B).

+ Addition of **fumaronitlile** reduce the β-hydride elimination product (styrene).
+ The coordination of fumaronitrile to the palladium dialkyl intermediate **precludes the availability of an open coordination site** on palladium required for β-elimination.
+ The electron-deficient nature of the olefin facilitated reductive elimination.

Scheme 44. Palladium-catalyzed coupling of 1-bromo-1-phenylethane (68) with tetramethylstannane and two possible reaction pathways for the proposed dialkyl palladium intermediate **69** (A: reductive elimination; B: β-hydride elimination).

Promotion of reductive elimination (Schwartz et al. *JACS* **1982**, *104*, 1310.)

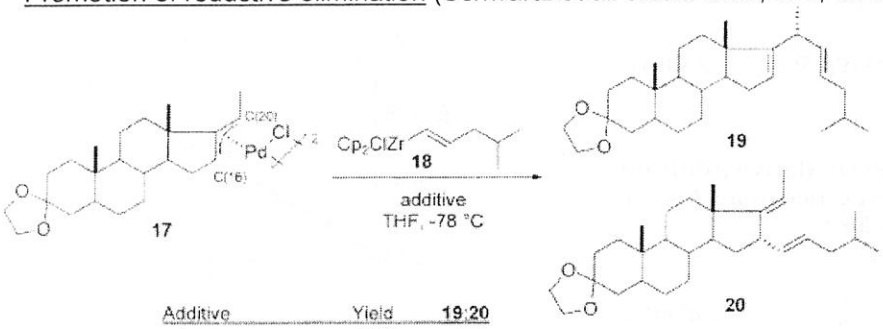

Additive	Yield	19:20	
none	51%	2:3	
PPh_3	0%	-	σ-donor ligand
	96%	>7:1	π-acceptor ligand

Scheme 17. Additive effects in the coupling of π-allyl palladium complexes with organozirconium species.

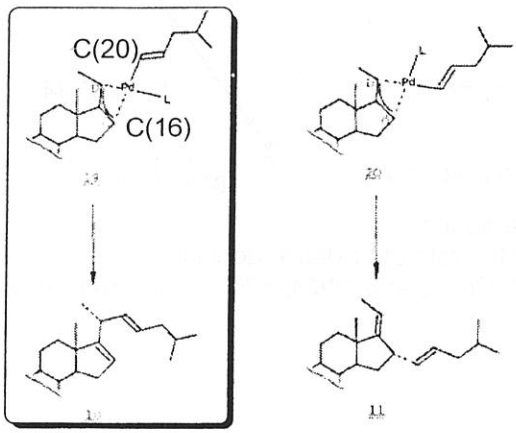

L = meleic anhydride

+ The author speculated that reductive elimination was facilitated using π-acceptor ligand meleic anhydride.
+ The weaker acceptor ligands trans to the more strongly donating (closer) terminus of the allylic ligand.

c) stabilization of catalyst

Rovis et al. *JACS* **2007**, *129*, 2718.

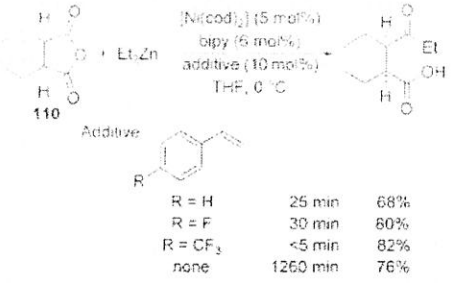

Scheme 75. Ni-catalyzed cross-coupling of *cis*-cyclohexanedicarboxylic anhydride (**110**) with diethylzinc in the presence of various styrene additives

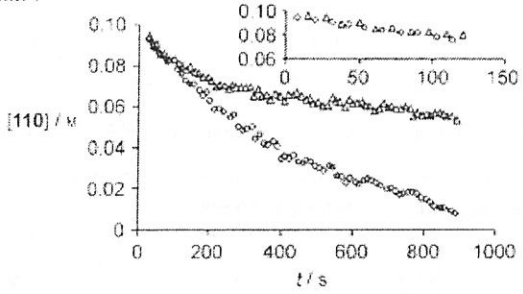

Figure 1. The concentration of succinic anhydride **110** versus time during Ni-catalyzed cross-coupling with diethylzinc in the presence (○) and absence (◇) of 4-fluorostyrene (see Scheme 74).

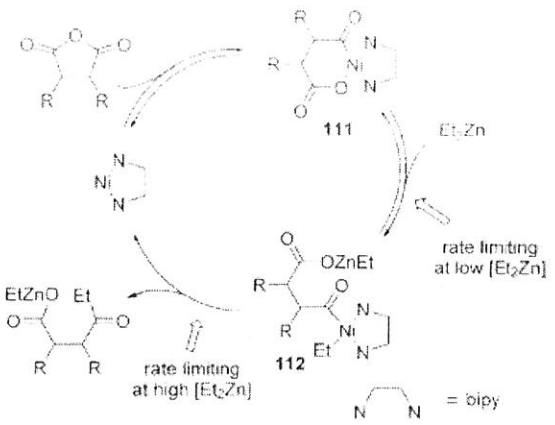

Scheme 74. Catalytic cycle of [Ni(cod)$_2$]–bipy-catalyzed cross-coupling of succinic anhydrides with diethylzinc

+ Figure 1 shows the slow deactivation of catalyst in the presence of styrene.
+ There was no effect on initial rate using styrene.

e) olefins in substrates

Pd catalyzed cycloisomerization (Trost et al. *JACS* **1994**, *116*, 4255.)

Scheme 1. Path for the Pd(+2)-Catalyzed Cycloisomerization of Enynes

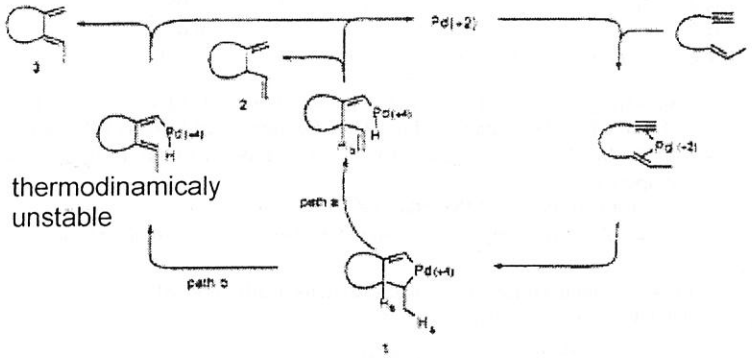

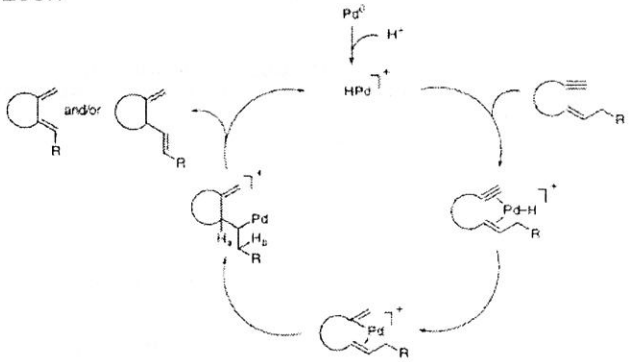

Scheme 2. Cycloisomerization of 1,6- and 1,7-enynes in a cycle involving HPd$^+$.

Another mechanism

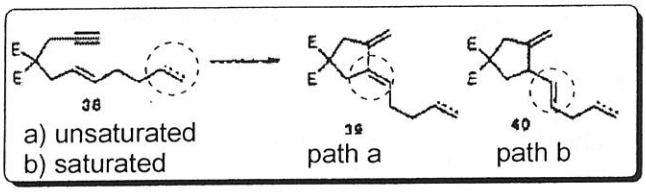

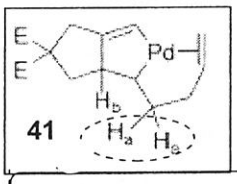

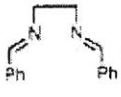

N,N-bis-(benzylidene)ethylenediamine

BBEDA

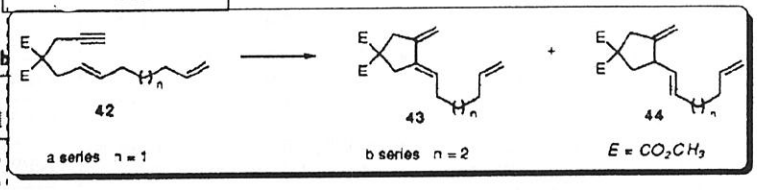

Table 1. Regioselectivity of Cycloisomerization of Enynes **38a** and **b**

entry	substrate	catalyst	ratio 39/40	yield
1	**38a**	$Pd(OAc)_2$	15:1	77%
2	**38a**	$[(o\text{-}CH_3C_6H_4)_3P]_2Pd(OAc)_2$	2.7:1	87%
3	**38a**	$(Ph_3P)_2Pd(OAc)_2$	1:2.1	73%
4	**38a**	BBEDA–$Pd(OAc)_2$	6.9:1	70%
5	**38b**	$Pd(OAc)_2$	only **40**	39%
6	**38b**	$[(o\text{-}CH_3C_6H_4)_3P]_2Pd(OAc)_2$	1:2.6	74%
7	**38b**	$(Ph_3P)_2Pd(OAc)_2$	1:2.9	78%

Table 1:
+ In entry 1-4, stronger binder phosphine (PPh_3) reversed the selectivity.
+ The geometry of intermediate **41** precluded the β-elimination of H_a, which lead to **40**.

Table 2. Regioselectivity of the Cycloisomerization of Dienynes **42a** and **b**

entry	catalyst	ratio 43/44 (% yield) from **42a**	from **42b**
1	$Pd(OAc)_2$	21:1 (76%)	1.1:1 (75%)
2	$[(o\text{-}CH_3C_6H_4)_3P]_2Pd(OAc)_2$	>20:1 (N.D.)[a]	1:1.6 (74%)
3	$(Ph_3P)_2Pd(OAc)_2$	2.7:1 (N.D.)	1:4.6 (81%)
4	$3Ph_3P$, $2Pd(OAc)_2$	1:2.3 (24%)	

[a] N.D. = not determined.

Table 2:
+ The length of tether is important.

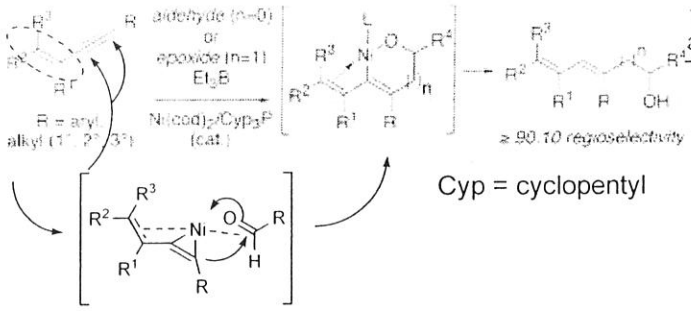

Cyp = cyclopentyl

Table 3. Effects of Alkene Directing Groups on Regioselectivity and Reactivity in Nickel-Catalyzed Alkyne Coupling Reactions[a]

reference alkynes (not alkene-directed)	*alkene-directed (this work)*	*effect of alkenyl group*
>20 : 1	1 : >20 (1a)	*reverses regioselectivity*
t-Bu, *t*-Bu (do not couple)	1 : >20 (1b)	*increases reactivity – and – controls regioselectivity*
2 : 1	1 : >20 (1d); >20 : 1 (1f)	*circumvents poor regioselectivity*

[a] Numbers indicate typical regioselectivity (Table 1 and refs 3d, g–i).

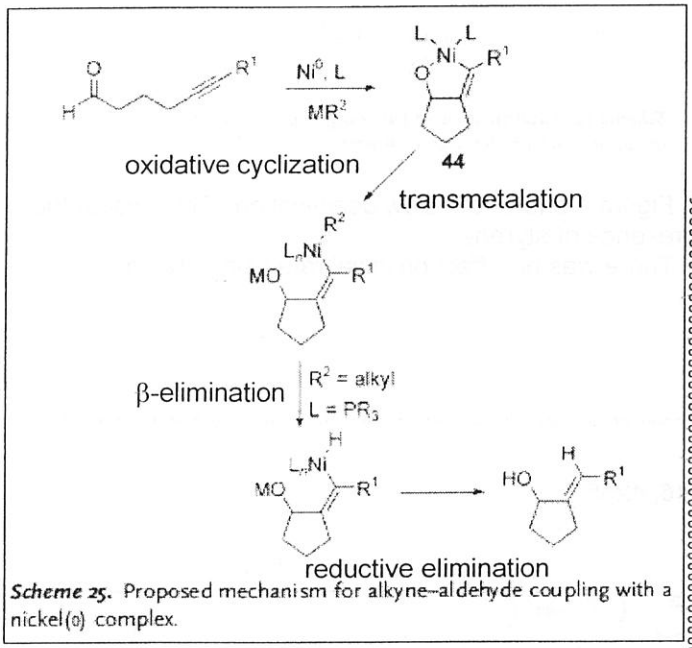

Scheme 25. Proposed mechanism for alkyne–aldehyde coupling with a nickel(0) complex.

Table 1. Directing effects of ~~tethered alkenes~~ *tethered alkenes*[a]

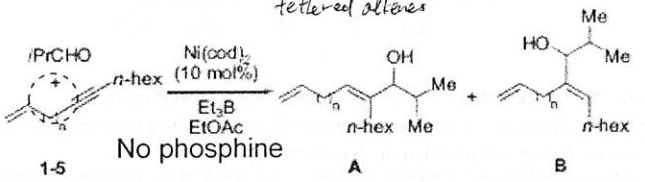

(3)

	Alkyne	*n*	Yield	Regioselectivity[b]
1	**1**	0	<5	n.d.
2	**2**	1	<5	n.d.
3	**3**	2	<5	n.d.
4	**4**	3	53[c]	>95:5
5	**5**	4	<5	n.d.
6	*n*-Pentyl–C≡C–*n*-hexyl	n.a.	28[c]	50:50

[a] Standard procedure: The alkyne (0.50 mmol) was added to a 0 °C solution of $Ni(cod)_2$ (0.05 mmol), *i*-PrCHO (1.00 mmol), and Et_3B (1.00 mmol) in EtOAc (0.5 mL), and the solution was allowed to stir 15 h at room temperature.
[b] Determined by ^1H NMR and/or GC.
[c] Some alkylative coupling (transfer of Et from Et_3B) also observed.

Table 4. Coupling reactions of chiral 1,6-enynes

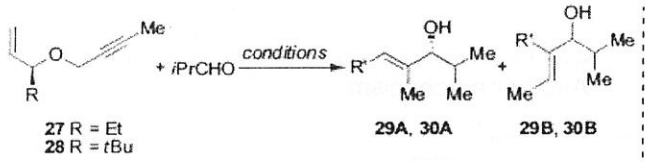

Entry	Enyne	Reaction conditions[a]	Products	A:B[b]	dr A[c]	dr B[c]
1	**27** (R=Et)	I	**29A, B**	>95:5	95:5	—
2		II		<5:95	—	45:55
3		III		55:45	50:50	45:55
4	**28** (R=*t*Bu)	I	**30A, B**	>95:5	>95:5	—
5		II		<5:95	—	42:58
6		III		51:49	45:55	42:58

[a] I: $Ni(cod)_2$ (10 mol %), Et_3B (200 mol %). II: Reaction conditions I+$PCyp_3$ (20 mol %). III: Reaction conditions I+PBu_3 (20 mol %).
[b] Based on isolated yields.
[c] Determined by ^1H NMR.

Table 4 :
+ Larger phosphine $PCyp_3$ gave **B**. But No diastereoserectivity (Entry 2).
+ No phosphine condition gave **A** with high diastereo selectivity. (Entry 1)

⟹ In **no phosphine** condition, **chiral center** was involved in C-C bond forming step.

Table 5. Coupling reactions of chiral, enantiomerically enriched 1,6-enynes[a] with ferrocenyl-containing phosphines

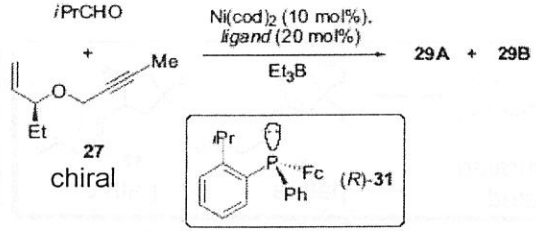

Ligand	A:B[b]	dr 29A (*R*:*S*)[c]	dr 29B[d]
(*R*)-**31**	48:52	30:70	28:72
(*S*)-**31**	55:45	66:34	68:32
$FcPPh_2$	54:46	56:44	48:52

[a] Enantiomerically enriched (>90% ee) **27** was used (Scheme 3).
[b] Based on isolated yields.
[c] Configuration of allylic alcohol stereogenic center.
[d] Relative stereochemistry not determined.

Table 5 :
+ (*S*)- and (*R*)- ligands gave almost same diastereoselectivity (face selectivity of aldehyde).

⟹ **27** of chiral center did not affect the selectivity.
Phosphine ligand was involved in C-C bond forming step.

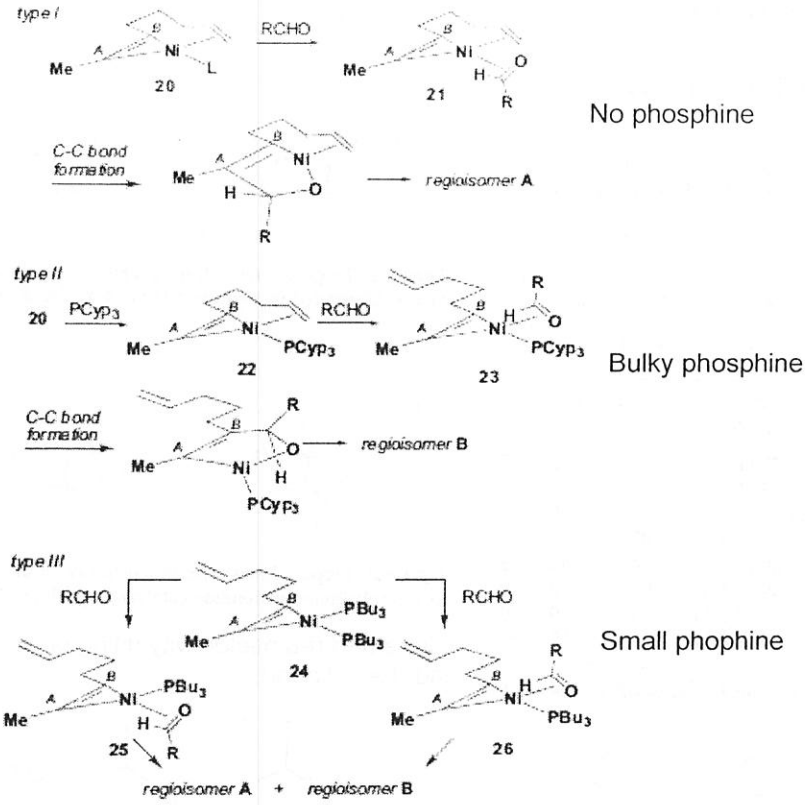

Scheme 2. Proposed mechanism

f) chiral olefin containing ligands

Review: *ACIE* **2008**, *47*, 4482.

i) First chiral olefin ligand (Cope et al. *JACS* **1962**, *84*, 3190.)

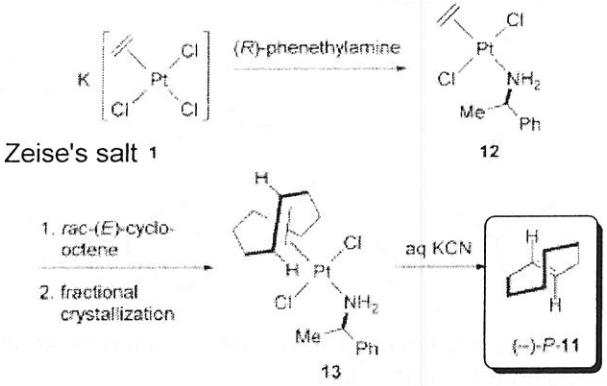

Merits of chiral olefin ligands is that they create a **chiral environment in proximity** to the metal.

Scheme 2. Synthesis of chiral (*E*)-cyclooctene ((−)-(*P*)-11) according to Cope et al.

ii) diene

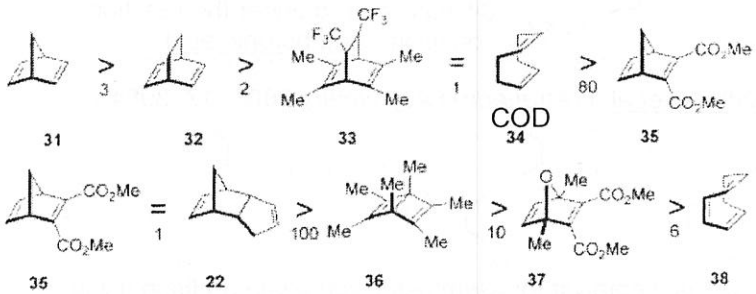

Stronger binder olefin ligands are ...
1) **electron deficient** derived from **electron-withdawing substituent** or **pyramidalization** which lower the π* LUMO of olefins.
2) rigid backbone

Scheme 9. Comparison of the stabilities of rhodium complexes with various chiral diene ligands.

Hayashi et al. (*JACS* **2006**, *128*, 5628.)

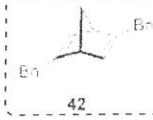

JACS **2003**, *125*, 11508.

42

Table 1. Rhodium-Catalyzed Asymmetric 1,4-Addition of Phenylboronic Acid to Substituted Maleimides **1**: Ligand Effect

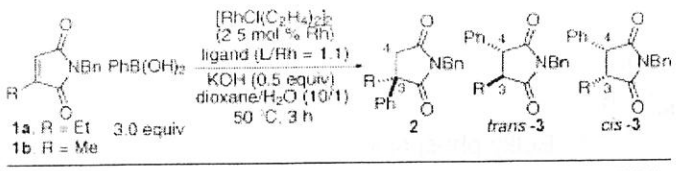

entry	1	ligand	yield (%)[a]	2/3[b] (trans/cis)	ee of 2 (%)	ee of 3 (%) (trans, cis)
1	1a	(*R,R*)-Bn-bod*	93	22/78 (1.6/1)	73	82, 97
2	1a	(*R,R*)-Ph-bod*	94	15/85 (1/2.3)	97	83, >99
3	1a	(*R*)-binap	99	85/15 (2.0/1)	96	68, 96
4	1a	(*R*)-H$_8$-binap	98	87/13 (2.3/1)	97	−19, 96
5	1b	(*R,R*)-Bn-bod*	94	20/80 (2.1/1)	84	82, 93
6	1b	(*R,R*)-Ph-bod*	94	11/89 (1/1.4)	93	79, 99
7	1b	(*R*)-binap	98	75/25 (2.1/1)	95	0, 96
8	1b	(*R*)-H$_8$-binap	98	81/19 (2.8/1)	96	−10, 94

[a] Combined yield of **2** and **3**. [b] Determined by ^{1}H NMR of the crude material.

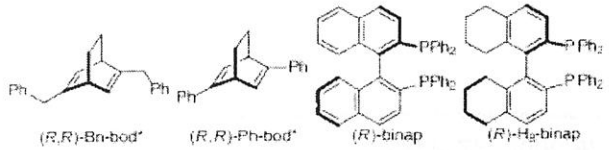

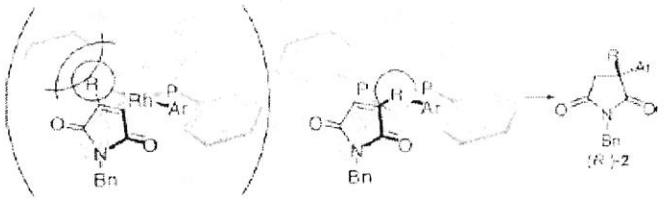

Figure 1. Proposed stereochemical pathway for the asymmetric 1,4-addition to a 3-substituted maleimide catalyzed by Rh/(*R*)-H$_8$-binap.

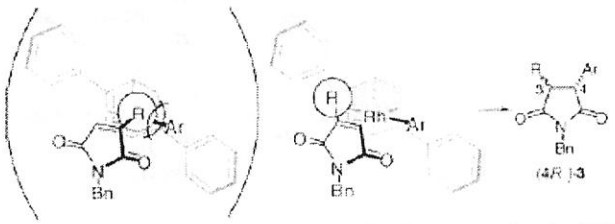

Figure 2. Proposed stereochemical pathway for the asymmetric 1,4-addition to a 3-substituted maleimide catalyzed by Rh/(*R,R*)-Ph-bod*.

+ Inversed regioselectivity using phosphine ligand and diene ligand.

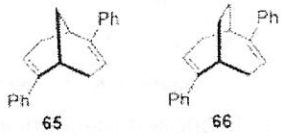

Other Hayashi's ligands

Carreira et al. (*JACS* **2004**, *126*, 1628.)

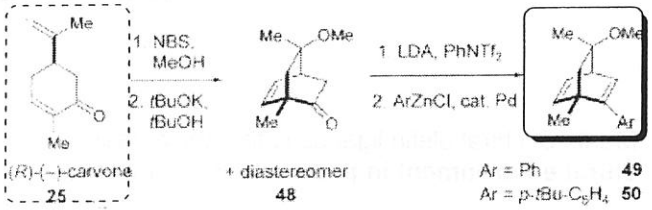

Scheme 12. Synthesis of the chiral bicyclo[2.2.2]octadienes **49** and **50** according to Carreira and co-workers. NBS: *N*-bromosuccinimide.

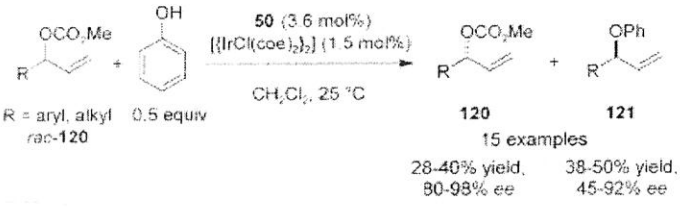

Scheme 28. Ir/diene-catalyzed kinetic resolution of allylic carbonates.

Grutzmacher et al. (*Organometallics* **2005**, *24*, 2997.)

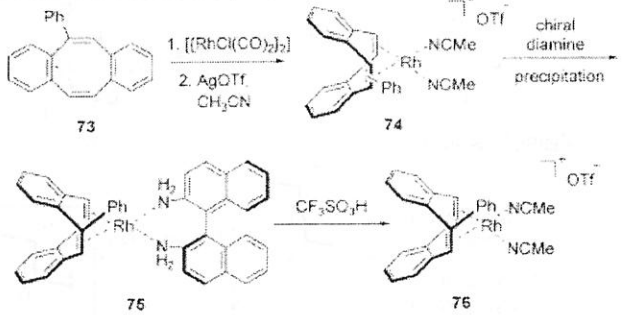

+ **76** is a catalyst for asymmetric conjugate addition using arylboronic acids.

Hayashi et al. (*OL* **2005**, *7*, 5889.)

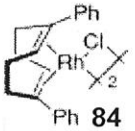

+ **84** is a catalyst for asymmetric conjugate addition using zinc reagent.
+ Racemization (dissociation of ligand) of **84** was ocurred under the reaction condition using boronic acid.

Trauner et al. (*Organometallics* **2005**, *24*, 2831.)

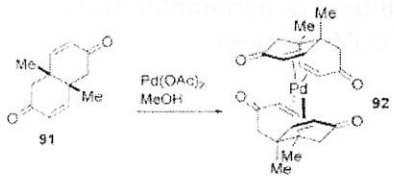

+ **91** is an **electron-deficient** olefin ligand.
+ **92** is enough to stable to be purified by column chromatography.
+ No asymmetric reaction catalyzed by **92** have been reported.

Widhalm et al. (*Tetrahedron Asymmetry* **2006**, *17*, 3084.)

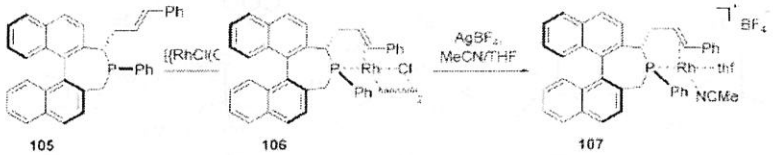

+ **107** is a catalyst for asymmetric conjugate addition using arylboronic acids.

Lin et al. (*JACS* **2007**, *129*, 5336.)

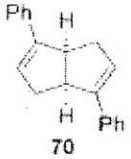

+ Ligand for highly enantioselective Rh-catalyzed arylation of imines with arylboronic acids.

iii) phosphine-olefin

chiral phosphine–olefins

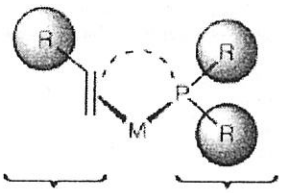

good chiral environment | high coordination ability

Hayashi et al. (*ACIE* **2005**, *44*, 4611.)

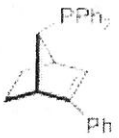

103

+ **103** is a catalyst for asymmetric conjugate addition using arylboronic acids.

Grutzmacher et al. (*Chem.Eur. J.* **2006**, *12*, 5849.)

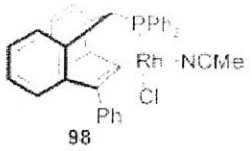

98

+ **98** is a catalyst for asymmetric conjugate addition using arylboronic acids.

Carreira et al. (*ACIE* **2007**, *46*, 3139.)

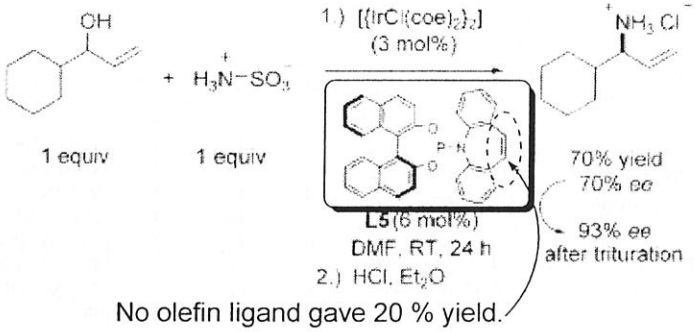

No olefin ligand gave 20 % yield.

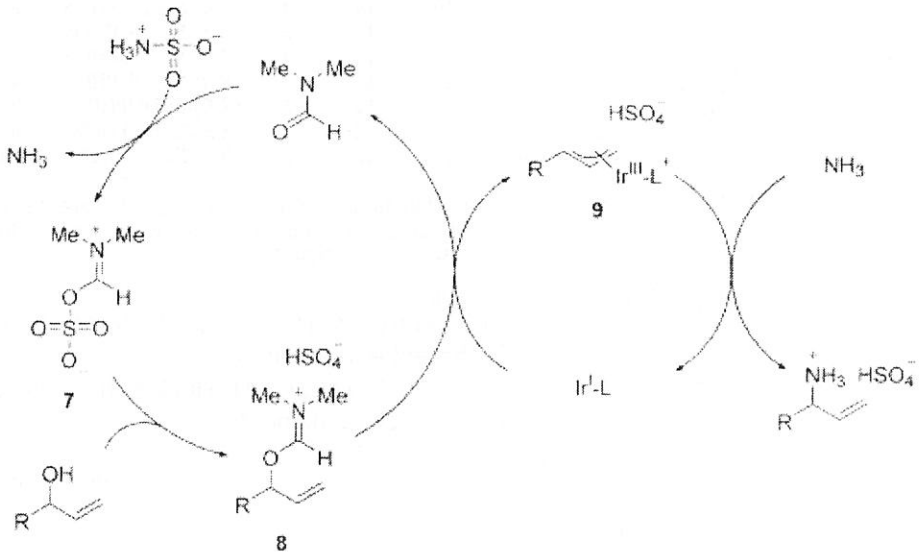

Scheme 3. Proposed working model. L = ligand.

---

iv) amine-olefin

Grutzmacher et al. (*Organometallics* **2005**, *24*, 3207.)

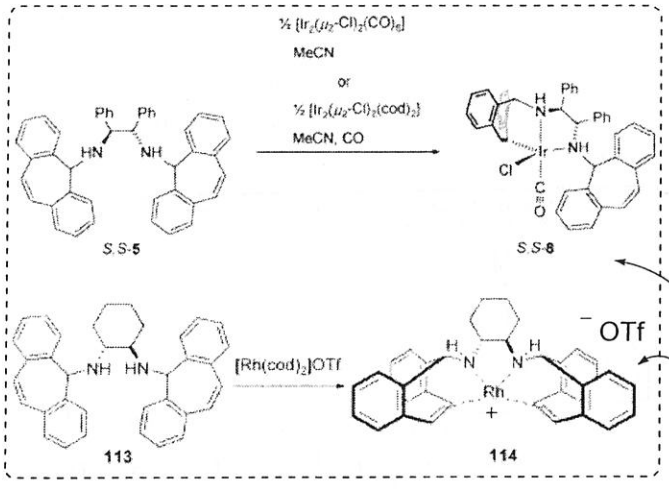

Scheme 5. Transfer Hydrogenation of Acetophenone Catalyzed by the Iridium Complex [IrCl(CO)(trop$_2$dpen)] ((*S*,*S*)-8)

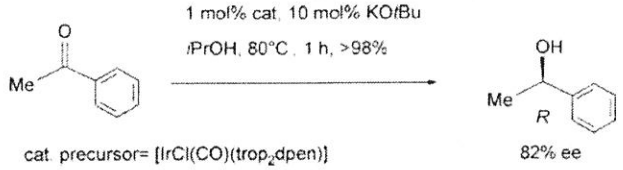

cat. precursor= [IrCl(CO)(trop$_2$dpen)]

82% ee

+ Complex **114** gave no reaction.

Proposed transition state for transfer hydrogenation of ketones

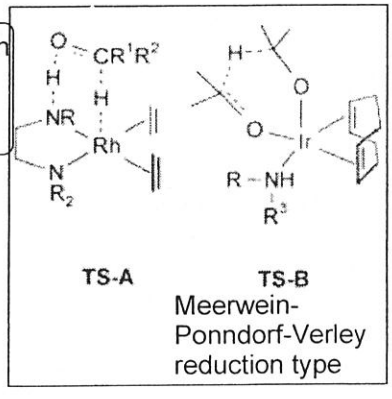

TS-A | TS-B

Meerwein-Ponndorf-Verley reduction type

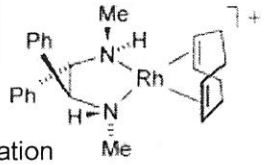

Catalyst for transfer hydrogenation

[Rh(*S*,*S*-dmpeda)(cod)]$^+$

Asymmetric Synergy between Chiral Dienes and Diphosphines in Cationic Rh(I)-Catalyzed Intramolecular [4 + 2] Cycloaddition (Mikami et al. *JACS* **2006**, *128*, 12648.)

Table 1. Enantioselective [4 + 2] Cycloaddition of 1a by Rh Catalysts Derived from a Variety of Rh–Diene Precatalysts

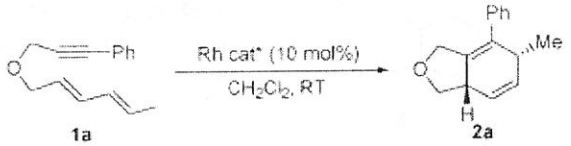

1a 2a

entry	Rh cat*	time	yield (%)[c]	ee (%)[d]
1[a]	$[Rh(COD_2](SbF_6)/(S,S)$BDPP	48 h	0	
2	[Rh{(*S,S*)-BDPP}(COD)]SbF_6	48 h	0	
3	[Rh{(*S,S*)-BDPP}(NBD)]SbF_6	4 h	81	0
4	[Rh{(*S,S*)-BDPP}]SbF_6	18 h	69	0
5[b]	$[RhCl(COD)]_2$/(*S,S*)-BDPP/$AgSbF_6$	30 min	89	0
6[b]	$[RhCl(COD)]_2$/(*S,S*)-CHIRAPHOS/$AgSbF_6$	40 min	87	0
7[b]	$[RhCl(COD)]_2$/(*R,R*)-DIOP/$AgSbF_6$	15 min	94	−2[e]
8[b]	$[RhCl(COD)]_2$/(*S*)-BINAP/$AgSbF_6$	20 min	70	9
9[b]	$[RhCl(COD)]_2$/(*R,R*)-Me-DUPHOS/$AgSbF_6$	5 min	99	13
10[b]	$[RhCl(NBD)]_2$/(*R,R*)Me-DUPHOS/$AgSbF_6$	5 min	88	0

[a] Rh:BDPP = 1:1.1. [b] Rh:ligand:$AgSbF_6$ = 1:1.1:2. [c] Isolated yield. [d] Enantiopurity was determined by chiral GC analysis on a CP-cyclodextrin-β-2,3,6-M-19. [e] Opposite configuration.

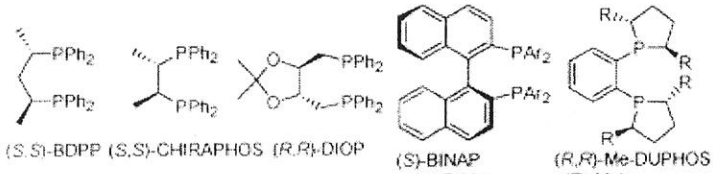

(*S,S*)-BDPP (*S,S*)-CHIRAPHOS (*R,R*)-DIOP (*S*)-BINAP (Ar=C_6H_5) (*S*)-DM-BINAP (Ar=3,5-$Me_2C_6H_3$) (*R,R*)-Me-DUPHOS (R=Me) (*R,R*)-Et-DUPHOS (R=Et)

Table 1:
+ In entry 9, 10, other symmetric olefin ligands gave different ee.

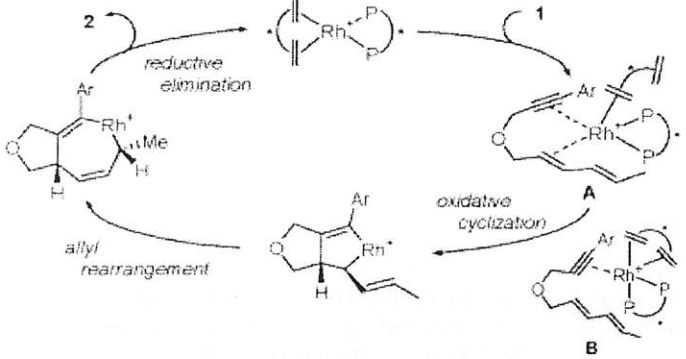

Figure 1. Plausible reaction mechanism.

Table 2. Enantioselective [4 + 2] Cycloaddition of 1a–e Catalyzed by Diphosphine–Rh Complexes Bearing Chiral Dienes

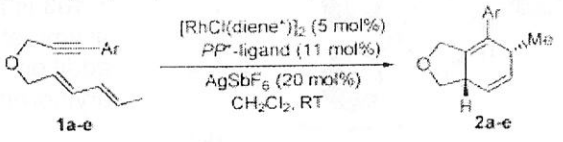

1a-e 2a-e

a: Ar = C_6H_5
b: Ar = *p*-OMe-C_6H_4
c: Ar = *p*-F-C_6H_4
d: Ar = *p*-Cl-C_6H_4
e: Ar = *p*-CF_3-C_6H_4

diene* =

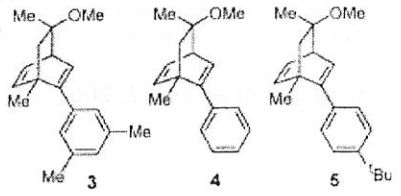

entry	substrate	diene*	PP* ligand	time	yield (%)[a]	ee (%)[c]
1	1a	3		30 min	91	26
2	1a	3	(*S,S*)-CHIRAPHOS	1 h	61	22
3	1a	3	(*S*)-BINAP	3 h	27	30
4	1a	3	(*R*)-BINAP	3 h	51	26
5	1a	3	(*S*)-DM-BINAP	30 min	81	29
6	1a	3	(*R*)-DM-BINAP	30 min	94	28
7	1a	3	(*R,R*)-Me-DUPHOS	40 min	90	88
8	1a	3	(*S,S*)-Me-DUPHOS	60 min	96	−9[d]
9[a]	1a	3	PPh_3	30 min	85	26
10	1a	4	(*R,R*)-Me-DUPHOS	2 h	82	91
11	1a	5	(*R,R*)-Me-DUPHOS	50 min	68	87
12	1b	4	(*R,R*)-Me-DUPHOS	2.5 h	51	81
13	1c	3	(*R,R*)-Me-DUPHOS	5 h	91	93
14	1a	3	(*R,R*)-Et-DUPHOS	2 h	99	95
15	1d	3	(*R,R*)-Et-DUPHOS	2 h	89	86
16	1e	3	(*R,R*)-Et-DUPHOS	1.5 h	97	98

[a] Rh:ligand:$AgSbF_6$ = 1:2.2:2. [b] Isolated yield. [c] Enantiopurity was determined by chiral GC analysis on a CP-cyclodextrin-β-2,3,6-M-19. [d] Opposite configuration.

Table 2:
+ In entry 7-9, (*S*, *S*)- and (*R*, *R*)-Me-DUPHOS gave different enantiomers.
⟹ (*R*, *R*)-Me-DUPHOS is the matched pair with chiral diene **3**.

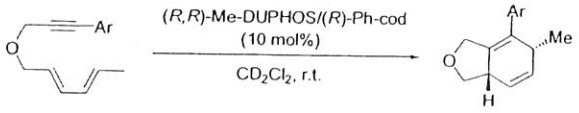

entry	Ar	time (h)	yield (%)	*ee* (%)
1[a]	Ph	16	65	9
2	Ph	7	90	93(88[b])
3	4-OMe-Ph	8	90	92(81[c])
4	4-Cl-Ph	6	95	87(86[b])
5	4-F-Ph	5	92	98(93[b])
6	4-CF_3-Ph	5	80	95

[a] Use of cod instead of Ph-cod. [b] Use of diene C_1-A instead of Ph-cod. [c] Use of diene C_1-B instead of Ph-cod.

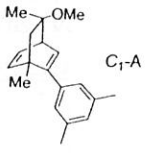

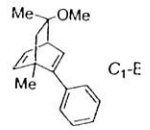

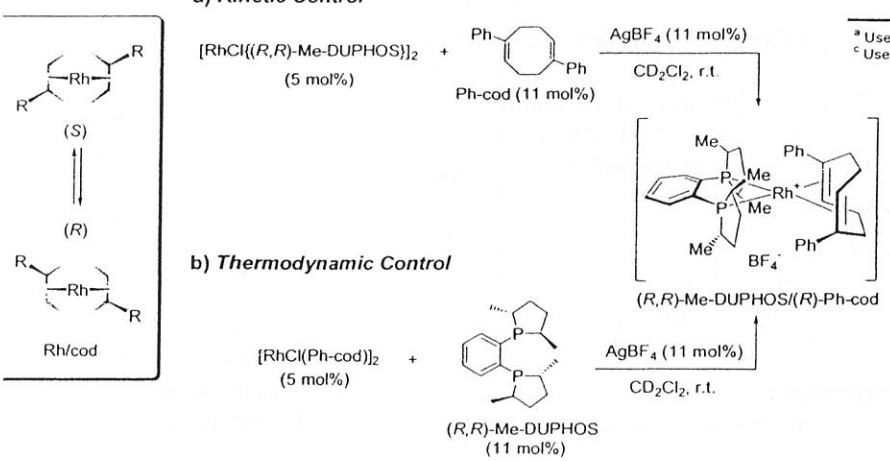

Scheme 4

Table 3

↘ In 2005, Hayashi et al. prepared Rh(R)-Ph-cod complex using (R)-BINAMINE. (See page 8.)

第93回有機合成シンポジウム講演要旨集より
(Mikami et al. 2008/06/12~13)

Other works using chiral diene ligands from 第93回有機合成シンポジウム講演要旨集 (2008/06/12~13)

Mikami et al.

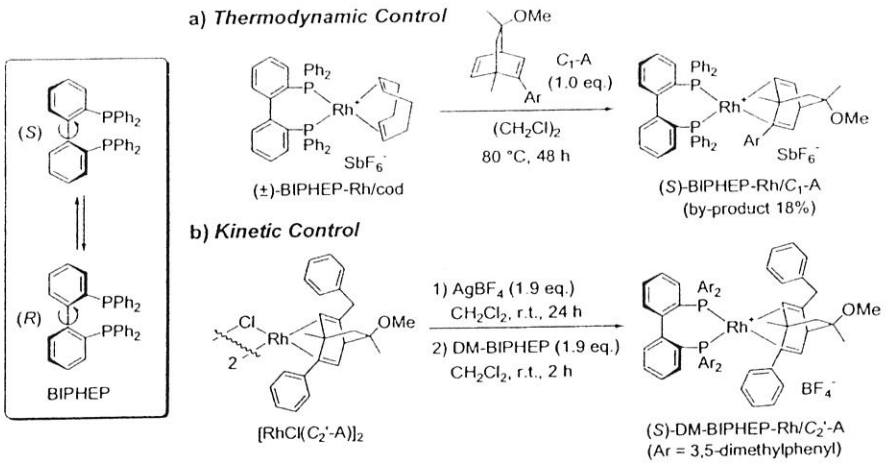

Scheme 1

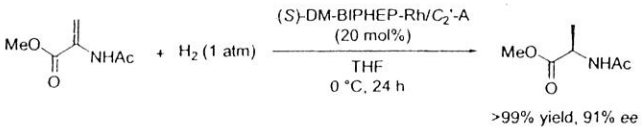

Scheme 2

· there was no racemization of catalyst. (no racemization of BIPHEP and no hydrogenation of diene ligand.)

Endo et al.

Figure 2. ジアミン配位子による金属外圏の制御

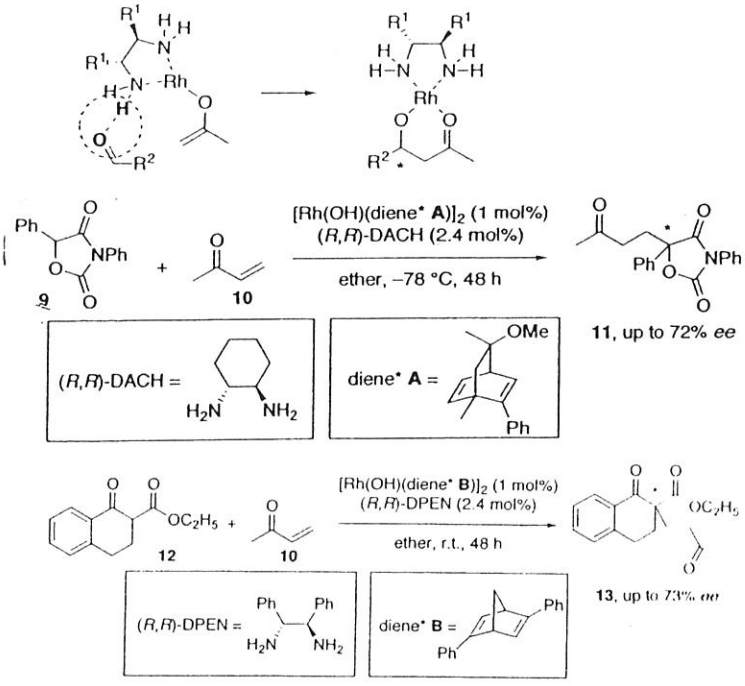

· In the absence of chiral diene ligand, the ee was 5 %.

· N-alkylated diamine ligand gave no reaction